Investigating the New Schiff Base
(E)-2-(((2-bromo-3-methylphenyl)imino)methyl)-4-methoxyphenol
Using Synthesis, XRD, DFT, FTIR spectroscopy, Hirshfeld, NBO, Frontier Molecular Orbitals, MEP and Electrophilicity-based Charge Transfer Analysis

[1]Abdurrahman Suhta*, [2]Ceren Çiçek, [1]Ufuk Çoruh, [2]Erbil Ağar and [3]Ezequiel M. Vazquez Lopez
[1]*Department of Physics, Faculty of Sciences, OndokuzMayıs University, 55139, Samsun, Turkey.*
[2]*Department of Chemistry, Faculty of Sciences, OndokuzMayıs University, 55139, Samsun, Turkey.*
[3]*Department of Inorganic Chemistry, University of Vigo, Vigo 36310, Galicia, Spain.*
*a.suhta@hotmail.com**

Summary: In this research, the title compound was synthesized and characterized using spectroscopic analyses like FTIR and XRD. The compound's structure was optimized using Density Functional Theory (DFT) at B3LYP method with 6-311++G(d,p) basis set. The experimental parameters obtained by XRD were found to agree well with the theoretically calculated parameters. The title compound was studied using several methods, including FMOs, MEP, Hirshfeld surface analysis, 2D fingerprint plots, net charges, Electrophilicity-based Charge Transfer (ECT), Natural Bond Orbital analysis and global chemical reactivity descriptors.

Introduction

Hugo Schiff, a German scientist and Nobel Prize laureate, initially synthesized Schiff bases in 1864 as a new class of organic compounds [1]. Schiff base ligands are significant due to their many advantageous qualities, such as their ability to change which gives high flexibility and leads to offer various donor groups. Functional variety leads to a wide range of coordination numbers, which are given by these readily accessible ligands that coordinate with various metals used in complex production [2]. The compounds of Schiff bases, which include the -C=N-double bond, are formed when an aldehyde or ketone reacts with a primary amine (Fig 1). These compounds known as Schiff base compounds can also be found as azomethines, imines, and anilines in some sources. Researchers are particularly interested in orthohydroxy Schiff base compounds because of their thermochromic, photochromic, and solvatochromic capabilities in several environments such as solvent and crystalline [3, 4].

Schiff base has garnered significant attention since its discovery depending on its important properties such as: biological, antibacterial, antifungal, biocidal, antiviral, antimalarial, and anticancer. So, it found applications that used in medicine, modern technologies, synthesis and chemical analysis [6-17]. Schiff base compounds also possess optoelectronic and electrical characteristics, thermal resistance, semiconductivity, liquid crystal behaviour, fiber forming abilities, and excellent photo- and electroluminescence characteristics [18, 19].

Theoretical techniques are used along with spectroscopic or experimental methods with the aim of predicting the spectral and geometric features of the compound. Between several theoretical methods, DFT is a relatively inexpensive and widely used method for getting information about the transition states, structure and energy values of compounds [20]. Furthermore, the DFT is very accurate method when used to predict the chemical analyses of molecules using spectroscopic analysis methods [11].

The synthesis, crystal structure, spectral characterization, and computational analyses of the title compound are presented in this paper. The title compound is a new compound and has not been studied previously. XRD was employed to identify the crystalline structure of the compound. The vibrations of FT-IR spectra that collected experimentally and calculated in other references are discussed in this paper. The nature of intermolecular interaction was investigated through Hirshfeld surface analysis, while 2D fingerprint diagrams and molecular surface lines offered a description of the percentage of bond interactions in the compound. The analysis of ECT, and the global and local chemical activity investigations were calculated using DFT. Furthermore, DFT computations were done with the aim of determining the optimized molecular structural parameters and HOMO-LUMO energies.
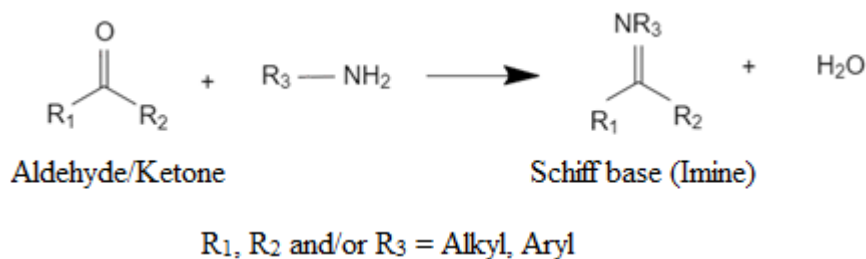
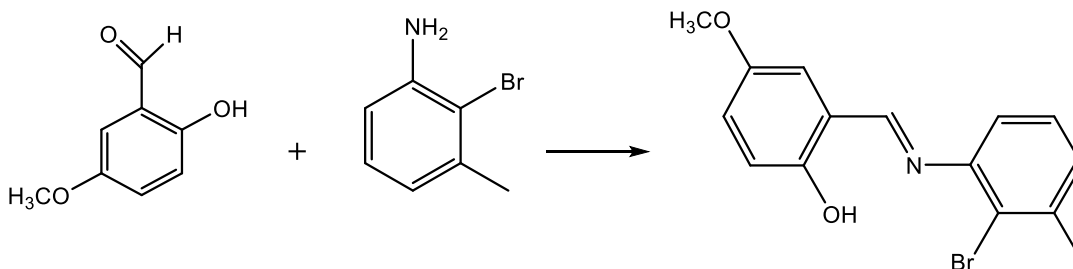Fig 1:   Synthesis of a Schiff Base in a General conformation [5].

Fig. 2:   Synthesis pathway of the title compound.

Experimental

The FTIR spectrum of the compound was obtained by Shimadzu FTIR-8900 spectrophotometer using KBr pellets in the region of 400-4000 cm^{-1}.

Synthesis and characterization

The (E)-2-(((2-bromo-3-methylphenyl)imino)methyl)-4-methoxyphenol was synthesized through refluxing mixed solutions of 2-Hydroxy-5-methoxy benzaldehyde (0,15 mg, 1,0 mmol) in ethanol (15 ml) and 2-bromo-3-methylaniline (0,19 mg, 1,0 mmol) in ethanol (15 ml). The reaction mixture was agitated for 5 hours while heating under reflux conditions, and Single crystals were formed by stepwise evaporation of an ethanol solution (70% yield, mp 359–361 K).

Crystal structure determination using XRD method

Bruker D8 Venture Photon 100 CMOS image plate diffractometer was utilized to collect the X-ray data at 100 K temperature. The w-scan technique was used, as well as graphite-monochromated Mo-K$_\alpha$ radiation (λ=0.7107300Å). As seen in Table 1, the result of crystal structure determinations and the refined parameters were displayed. The crystal structure of the compound was solved using direct techniques in SHELXS [21], refined using full-matrix least-squares methods on F^2 in SHELXL-97 [22], and performed with WinGX [23] program suite. ORTEP-III [24], Mercury [25], and Platon [26] software programs were used to do molecular geometry calculations and to draw the compound. All non-hydrogen atoms of the complex were refined anisotropically while H atoms in the geometrical sites were included without refining. The crystallographic information of the compound is presented in Table 1. The Cambridge Crystallographic Data Centre can provide crystallographic information and final refinement parameters of the title compound with reference number (CCDC: 2174889). In order to get copies of the data free of cost, an application must be submitted to CCDC 12 Union Road, Cambridge CB21 EZ, UK. (Fax: (b44) 1223 336-033; Email: data_request@ccdc.cam.ac.uk).

Computational procedures

DFT method was employed to do all of the quantum computations. The optimization process of the compound was done to study the molecular structure using DFT method at B3LYP/6-311++G(d, p) basis set by Gaussian 09 software [27] and GaussView 6 [28] molecular visualization software. B3LYP is a hybrid functional in computational chemistry that combines the benefits of the Becke three-parameter hybrid functional (B3) for the exchange part with the Lee-Yang-Parr (LYP) correlation functional and widely used to calculate molecular properties such as energies, structures, and chemical reactivity [29, 30]. It is cost-effective approach and considered to be very operative in giving satisfactory calculated geometries, especially in organic compounds. Crystal Explorer program 3.1 was used to generate Hirshfeld surface and 2D fingerprint plots to visualize the molecular interactions [31].

Table-1. Refined crystal data for the studied molecule

|	
CCDC deposition number	2174889
Chemical formula	$C_{15}H_{14}BrNO_2$
Formula weight	320.18
Wavelength	Mok_a, λ=0.7107300 Å
Temperature	100 K
Cryst. system	Orthorhombic
Space group	Pbca
Cryst. colour	Yellow
a, b, c (Å)	11.2243(6), 8.4147(5), 28.1626(15)
α, β, γ (°)	90, 90, 90
Volume	2659.9(3) Å³
Z	8
Density	1.599 Mgm⁻³
μ	3.088 mm⁻¹
Absorpt. correction	Multi-scan
F₀₀₀	1296
Diffractometer/ meas. method	Bruker D8 Venture Photon 100 CMOS /f and w scans
θ range (°)	2.320≤ θ ≤28.306
Index ranges	-14≤h≤14, -11≤k≤8, -36≤l≤37
T_{min}, T_{max}	0.5938, 0.7457
Reflections collected	20075
Independent/observed reflections	3298, 2660
R_{int}	0.043
Final R indices [I>2σ(I)]	R_1=0.0292, wR_2=0.0563
R indices (all data)	R_1=0.0445, wR_2=0.0602
Data/restraints/parameters	3298/0/172
Goodness of fit on F^2	1.076
$Δρ_{max}$, $Δρ_{min}$ (e/Å³)	0.317, -0.371

(a)

(b)
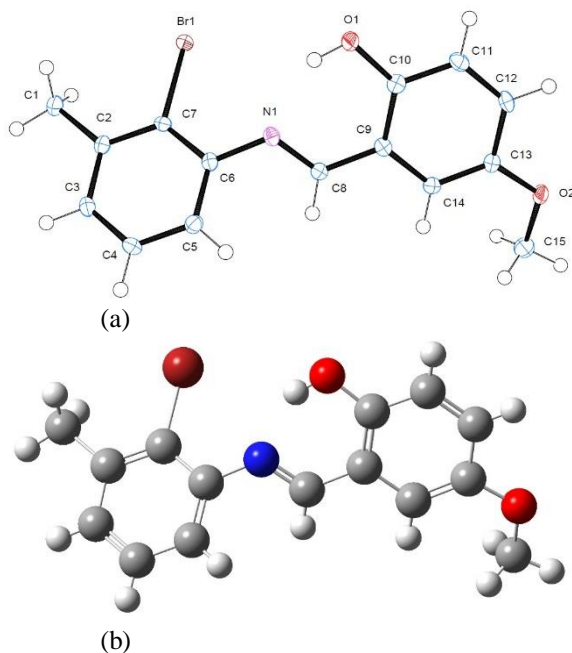
Fig. 3: (a) Ortep-III molecular drawing. (b) Optimized structure obtained by DFT.

Results and discussion

Crystal structure and optimized geometry

The 3-dimensional structure view of the chemical compound is given in Fig. 3 with labels of heavy atoms and done by Ortep- III program packet. XRD analysis shows that the title compound has orthorhombic crystal system with Pbca space group. The unit cell parameters are: a = 11.2243 (6)Å; b = 8.4147 (5)Å; c = 28.1626 (15)Å; α = 90°; β = 90°; γ = 90°; Z = 8; V = 2659.9(3)Å³. The main differences between the bond structure parameters that calculated theoretically and experimentally were presented in Table S2 (Supporting Information).

Fig 4 illustrates that the compound at N1 atom possesses tautomeric property. Tautomerism is caused by proton transfer within a molecule in O-hydroxy Schiff bases. This proton transfer results two tautomeric structures formed by two different hydrogen bonds which are N⋯H-O in the form of enol-imine and O⋯H-N in the form of keto-amine [32]. In the enol-imine form, the C10-O1 bond is single while in C8-N1 is double. In the keto-amine, the C10-O1 bond is double while in C8-N1 is single (Fig. 4).
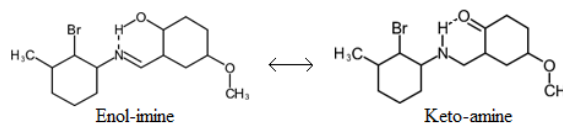

Fig. 4: Tautomeric forms of the title compound.

O1–C10 (1.353(2)) and N1–C8 (1.286(2)) bonds display single-bond and double-bond characteristics, respectively, indicating that the form of enol-imine is preferred over the form of keto-amine in the studied molecule. In addition, because the H1 atom is found near the O1 atom, the title compound is included in the solid state as an enol-imine form. Similar results have been reported showing acceptable agreement with the calculated results of the studied compound: (O3 C5 = 1.328(3)Å, N2 C7 = 1.270(3)Å [33]) and (O1 C6 = 1.348(2)Å, N1 C6 = 1.283(3)Å [34]). Also the bond distances of Br1-C7, C6-N1 and O2-C13 are calculated at 1.9025(18)Å, 1.414(2)Å and 1.374(2)Å respectively, which have good agreement with another studies: Br1-C11= 1.899(3)Å [35], Br01-C7= 1.902 (3)Å [36], Br2-C12= 1.904 (6)Å [37], C8-N2=1.4203 (19)Å [32], C9-N1=1.3956(16)Å [38], C9-N1=1.423(5)Å [39], O10-C6= 1.3677 (18)Å [40], O4-C9= 1.3640 (18)Å [41], O4-C9= 1.372 (2)Å [42].

The two phenyl rings (Ph1: C2/C7) and (Ph2: C9/C14) have the planar conformation in the crystal structure. The experimental results measured by XRD displayed dihedral angle between Ph1 and Ph2 rings at 42.28(0.06)°. The crystal structure of the studied molecule exhibits strong intramolecular hydrogen bonding which keeps the crystal structure stable (Table 2). Fig 5 and Table-2 illustrate that crystal packing of the studied molecule is mainly stabilized by the intermolecular C15-H15B⋯O1ⁱⁱ and C15-H15C⋯O2ⁱⁱⁱ hydrogen bonds.
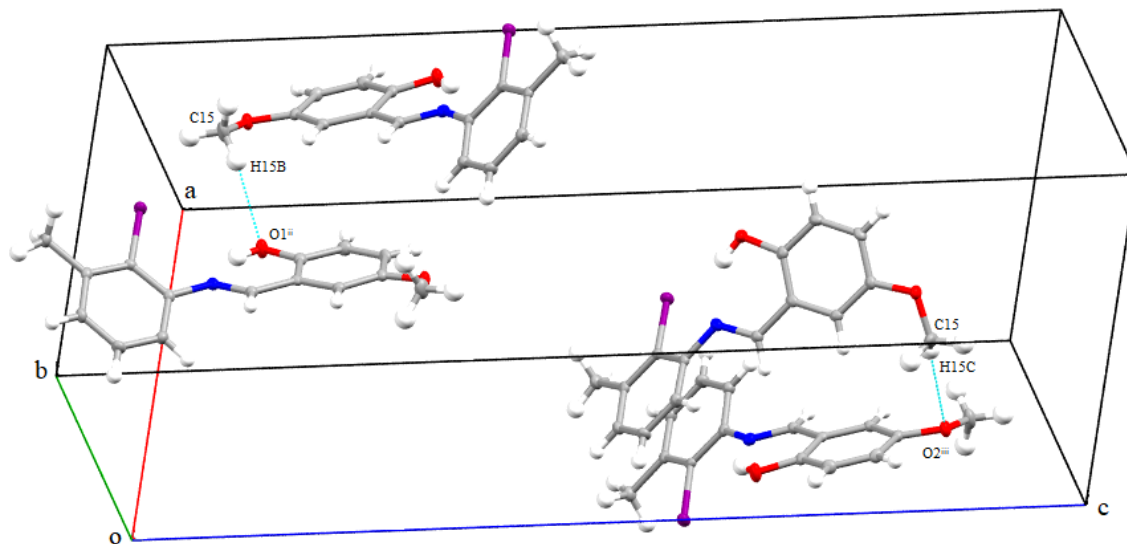
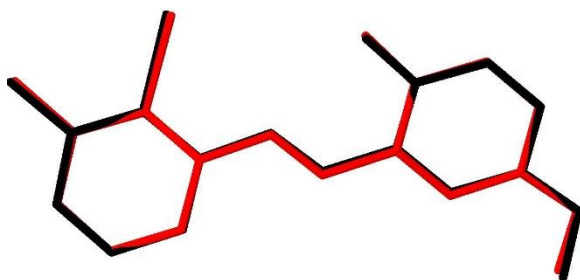Fig. 5:   Crystal packing of the studied compound.

Fig. 6:   Overlap between the structure obtained by XRD (red colour) and optimized structure (black colour) of (E)-2-(((2-bromo-3-methylphenyl)imino)methyl)-4-methoxyphenol.

Table-2: H-bond lengths (Å) and angles (°).

D—H⋯A	D—H	H⋯A	D⋯A	D—H⋯A
O1—H1⋯N1	0.84	1.87	2.606 (2)	146
C15—H15B⋯O1^{ii}	0.98	2.60	3.532 (3)	158
C15—H15C⋯O2^{iii}	0.98	2.61	3.347 (3)	132
Symmetry codes, i: −x+2, y−1/2, −z+1/2; ii: x−1/2, y, −z+1/2; iii: −x+3/2, y+1/2, z.				

The consistency among empirical and theoretical parameters were matched quantitively by the root mean square deviation analysis (RMSD) for the studied complex and displayed in Fig 6. As a result of RMSD, the superimposition of atomic positions between the molecular geometries observed crystallographically and the optimized molecule was calculated at 0.109Å. As seen from the previous analysis, the observed and calculated geometric parameters are compatible together. Theoretical parameters differ from empirical parameters for several reasons: due to the effects of neglect in the gas phase and due to molecular interactions that are not taken into account in theoretical techniques.

Hirshfeld surface analysis

Hirshfeld surface analysis (HSA) is based on determining the space occupied of the molecule inside the crystal where the electron density of this molecule equals the others and contributes to giving information about the interactions between the molecules inside crystals. HS is defined by two factors which are d_e and d_i. d_{norm} refers to the normalized contact distance and identifies important regions for intermolecular interactions and its value reflects whether vdW separations are shorter or longer than intermolecular interactions. The d_{norm} indicated in Eq. 1 can be calculated by defining Van Der Waals radius (r^{vdw}), d_i and d_e. HS and 2D fingerprint plots were created with CrystalExplorer21 software [43-45].

$$d_{norm} = \frac{d_i - r_i^{vdw}}{r_i^{vdw}} + \frac{d_e - r_e^{vdw}}{r_e^{vdw}} \qquad (1)$$

The d_{norm}, d_e, d_i, shape index and curvedness are -0.0853 to 1.0635, 1.0443 to 2.4825, 1.0448 to 2.4916, -1 to 1 and -4 to 4 Å, respectively. Fig 7 shows the maps generated by HSA. The HS plot mapped with d_{norm} was presented with various colors, where red and blue indicate to shorter contacts and longer contacts, and white indicates to contacts around the vdW separation. The dark red dots indicate stronger hydrogen bonds than light red dots. The dominant forces between all 2D fingerprint plots are related to H...H and H...C/C...H contacts with 38% and 29%, respectively. The other important contacts presented in Fig. 9 are O...H/H...O (13.7%), Br...H/H...Br (12.3%), C...C/C...C (2%), N...C/C...N (1.7%), N...H/H...N (1.3%), Br...C/C...Br (0.8%) and O...C/C...O (0.3%). These interaction forces make the structure of molecules stable.

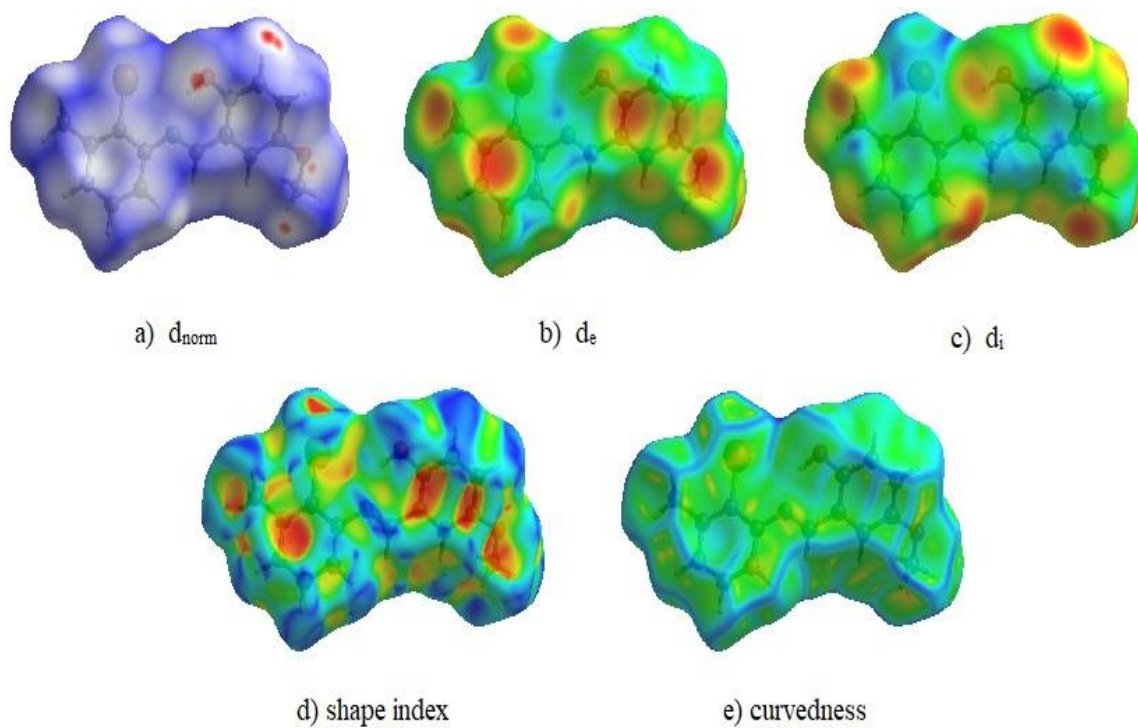a) d_{norm}

b) d_e

c) d_i

d) shape index

e) curvedness

Fig. 7: HS mapped with d_{norm}, d_e, d_i, shape index and curvedness of studied molecule.
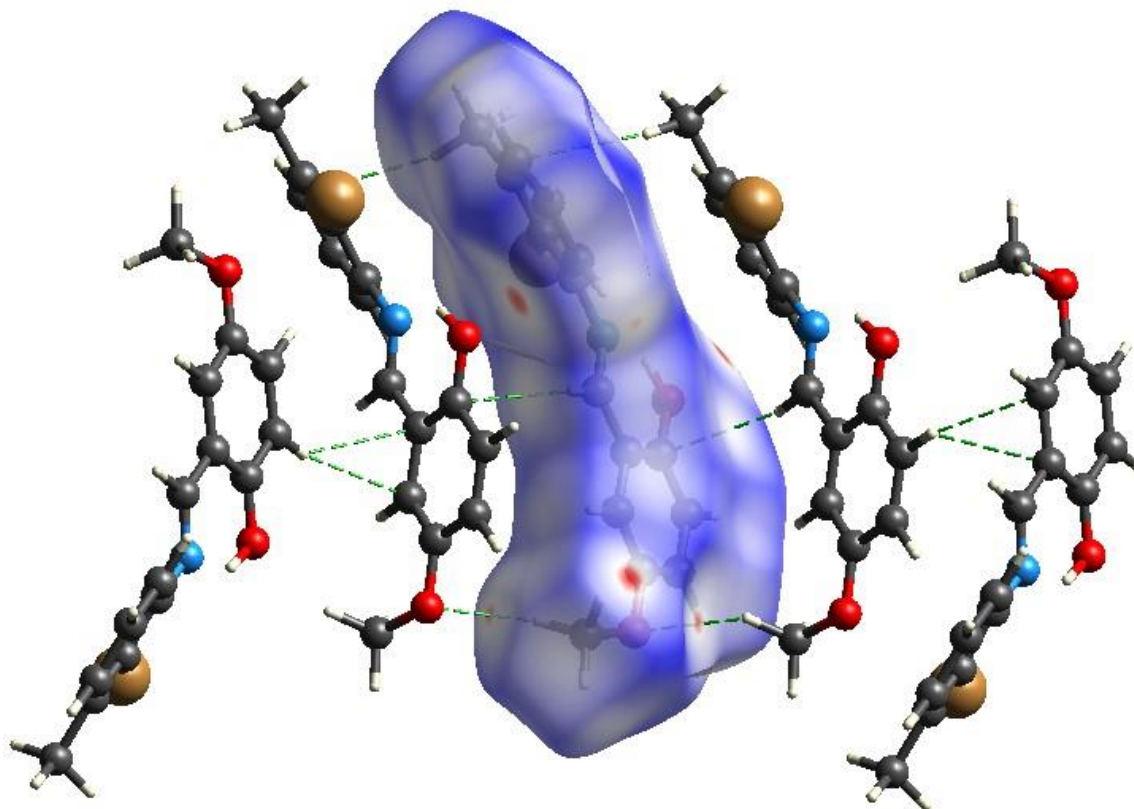

Fig. 8: HS mapped with d_{norm} to visualize the interactions between molecules.
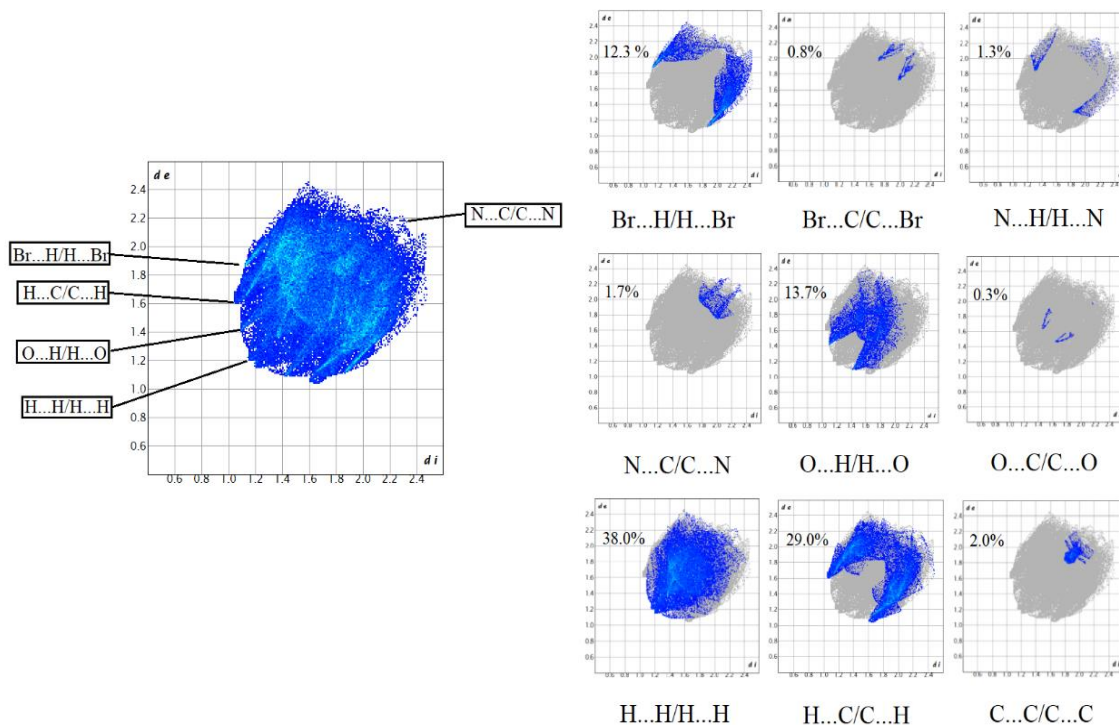
Fig. 9:   Fingerprint plots showing interactions of the title molecule.

The natural bond orbital analysis

The analysis of natural bond orbitals is a rapid technique to identify electronic structural features. It's also used for analysing conjugative interactions and charge transfer in molecules, as well as a handy tool for measuring intramolecular and intermolecular bonding interactions [46].

The NBO analysis was implemented with the method of DFT at the same basis sets to analyze the donor (i)-acceptor (j) bond interactions of the studied compound. The stabilization energy (E (^{2})) was calculated using Equation (2). The interaction of donor-acceptor within molecules, the energy of hyperconjucative interactions (E (^{2})), the energy difference between donor and acceptor i and j, percentage electron density, and the Fock matrix element between i and j NBO orbitals are calculated and presented in Table 3.

$$E^{(2)} = \Delta E_{ij} = q_i \frac{F(i,j)^2}{E_j - E_i} \qquad (2)$$

where q_i and $F(i,j)$ represent the donor orbital occupancy and off-diagonal NBO Fock matrix element. E_i , E_j represent diagonal elements orbital energies [47].

According to NBO study, the structure is a form of total Lewis structure for crystal with 97.982% (core, 99.974%; valance Lewis 96.681%) and total non-Lewis with 2.018% (Rydberg non-Lewis, 0.148%; Valence non-Lewis, 1.870%).

By increasing the E(^{2}) value, the intensity of interaction between donors and acceptors becomes bigger which means that the greater direction of donating electrons from donors to acceptors, the higher range of conjugation of the entire system. The delocalization of π electrons π(C12-C11)→π*(C10-C9), π(C5-C4)→π*(C6-C7) and π(C6-C7)→π*(C5-C4) possess stabilization energies at 20.48, 23.38 and 16.22 Kcal/mol, respectively. The overlap between σ(Br-C), σ(N-C), σ(O-C), σ(C-C) and σ*(C-C), σ*(N-C), σ*(Br-C) bond orbitals form the molecular interaction that make the system stable. According to Table 3, the overlap between the lone pair LP O2 orbital and π*(C13-C14) has the highest energy at 27.66 Kcal/mol. It is clear that the stability of the studied compound can be attributed to extended conjugation and charge transfer within the molecule. Moreover, the existence of the compound in the solid state is mostly related to hyperconjugative interactions and hydrogen bonds [48].

Table 3: Stabilization energies E(^{2}) calculated using DFT between the selected orbitals.

Donor(i) (Occupancy)	Bond A-B	ED$_A$,%; ED$_B$,%[a]	Acceptor(j) (Occupancy)	Bond A-B	ED$_A$,% ED$_B$,%	E(^{2})[b] (Kcal/mol)	E$_j$-E$_i$[c] (a.u.)	(Fij)[d] (a.u.)
BD Br1-C7 (1.98498)	σ	51.34; 48.66	BD* C5-C6 (0.02979)	σ*	51.30; 48.70	3.34	1.21	0.057
BD Br1-C7 (1.98498)	σ	51.34; 48.66	BD* C2-C3 (0.02281)	σ*	48.79; 51.21	3.29	1.22	0.057
BD N1-C6 (1.98218)	σ	58.76; 41.24	BD* N1-C8 (0.01173)	σ*	40.57; 59.43	1.11	1.38	0.035
BD N1-C6 (1.98218)	σ	58.76; 41.24	BD* C5-C6 (0.02979)	σ*	51.30; 48.70	1.38	1.34	0.039
BD N1-C8 (1.98678)	σ	59.43; 40.57	BD* N1-C6 (0.02678)	σ*	41.24; 58.76	1.24	1.31	0.036
BD N21-C8 (1.98678)	σ	40.57; 40.57	BD* C6-C7 (0.03450)	σ*	50.16; 49.84	2.07	1.43	0.049
BD O1-C10 (1.99422)	σ	66.26; 33.74	BD* C12-C11 (0.01309)	σ*	50.13; 49.87	1.47	1.51	0.042
BD O1-C10 (1.99422)	σ	66.26; 33.74	BD* C10-C11 (0.02201)	σ*	49.48; 50.52	0.52	1.48	0.025
BD O2-C13 (1.99262)	σ	67.10; 32.90	BD* C5-C19 (0.01309)	σ*	50.13; 49.87	1.40	1.48	0.041
BD O2-C13 (1.99262)	σ	67.10; 32.90	BD* C9-C14 (0.01847)	σ*	48.95; 51.05	1.22	1.44	0.037
BD C5-C6 (1.96723)	σ	48.70; 51.30	BD* Br1-C7 (0.03821)	σ*	48.66; 51.34	5.00	0.79	0.056
BD C5-C6 (1.96723)	σ	48.70; 51.30	BD* N1-C6 (0.02678)	σ*	41.24; 58.76	1.02	1.13	0.030
BDC12-C11 (1.71701)	π	48.62; 51.38	BD* C10-C9 (0.43375)	π*	55.00; 45.00	20.48	0.28	0.071
BD C5-C4 (1.67784)	π	51.62; 48.38	BD* C6-C7 (0.44447)	π*	54.27; 45.73	23.38	0.26	0.072
BD C6-C7 (1.66502)	π	45.73; 54.27	BD* C5-C4 (0.33597)	π*	48.38; 51.62	16.22	0.30	0.063
LP Br1 (1.93791)	n	-	BD* C6-C7 (1.93791)	π*	54.27; 45.7	9.35	0.31	0.053
LP O2 (1.86448)	π	-	BD* C13-C14 (0.35828)	π*	51.35; 48.65	27.66	0.34	0.092
CR N1 (1.99937)	σ	-	BD* C5-C6 (0.02979)	σ*	51.30; 48.70	0.65	14.72	0.088

[a] Percentage electron density of atom A and atom B.

[b] E (^{2}) Energy of hyperconjucative interactions.

[c] Energy difference between donor and acceptor i and j NBO orbitals.

[d] F(i, j) is the Fock matrix element between i and j NBO orbitals.

Frontier molecular orbitals

Frontier molecular orbitals (FMOs) are important in the chemical, electrical, and optical characteristics of molecular orbitals. The energy gap (Eg) can impact the biological activity of a molecule. A high energy gap (Eg) leads to low reactivity and chemical stability, while a small gap improves biological activity through charge transfer [49]. E$_{HOMO}$ reflects the molecule's ability to donate electrons, while E$_{LUMO}$ indicates the molecule's ability to accept electrons. [50].

The plots of frontier orbitals that show HOMO and LUMO are given in Fig. 10 to understand the bonding characteristic of the studied molecule. The Energy gap (Eg=E$_{LUMO}$-E$_{HOMO}$) is measured to be 3.72905 eV. This value is comparatively high, which suggests that the studied compound is chemically stable and has low reactivity [51].

Depending on Koopmans' theorem [52], ionization potential (I) and electron affinity (A) are calculated as below,

$$I = -E_{HOMO} \tag{3}$$
$$A = -E_{LUMO} \tag{4}$$

The global chemical reactivity parameters such as: the calculation of electronegativity (χ), the chemical potential (μ) which represents the force of an electron attached to the atom, chemical hardness (η) which allows determining the resistance of redistribution of electrons in the molecule, the softness (s) and the electrophilicity index (w) which determines the ability to accept chemical species for electrons are presented in Table 4 and can be determined as following equations [53],

$$\chi = \frac{(I+A)}{2} \tag{5}$$

$$\mu = -\frac{(I+A)}{2} \tag{6}$$

$$\eta = \frac{(I-A)}{2} \tag{7}$$

$$s = \frac{1}{2\eta} \tag{8}$$

$$w = \mu^2 / 2\eta \tag{9}$$

Net charges

Atomic charges calculation is significant in determining the properties and behavior of a molecular structure. The charges distribution on the atoms can be used to define the composition of donor and acceptor pairs in the compound [54, 55]. In this study, MPA (Mulliken population analysis) and NPA (natural population analysis) were done by DFT in gas phase. The MPA and NPA were used to calculate the atomic charge values by determining the electron population of each atom [56]. The difference between MPA and NPA is that in MPA, the charges are divided among the atoms equally whereas NPA considers the density of electron and polarization effect [57].

The results of MPA showed that atoms with negative charges such as C1, C3, C5, C14, C15, O1, O2 and N1 are reactive sites for the electrophilic attack, while atoms with positive charges such as C2, C4, C6, C7, C8, C9, C10, C11, C12, C13 and Br1 are reactive sites for nucleophilic attack (Table 5). Hydrogen atoms have a positive charge, making them acceptors. The results of atomic charges help interpret and predict the hydrogen bond region and the reactivity of chemical systems. The studied compound reveals more electrophilic nature than nucleophilic nature.

Table-4. Energy values of the studied molecule calculated by DFT.

Calculated energies	
E_{HOMO} (eV)	-5.90052
E_{LUMO} (eV)	-2.17147
I (eV)	5.90052
A (eV)	2.17147
E_g (eV)	3.72905
χ (eV)	4.035995
μ (eV)	-4.035995
η (eV)	1.864525
s $(eV)^{-1}$	0.268165
w	4.368205

(Ground state)
HOMO= -5.90052 eV

LUMO(+2)= -0.48164 eV

HOMO(-1)= -6.62489 eV

LUMO(+1)= -0.75049 eV

HOMO(-2)= -6.93129 eV

LUMO= -2.17147 eV
(First exited state)
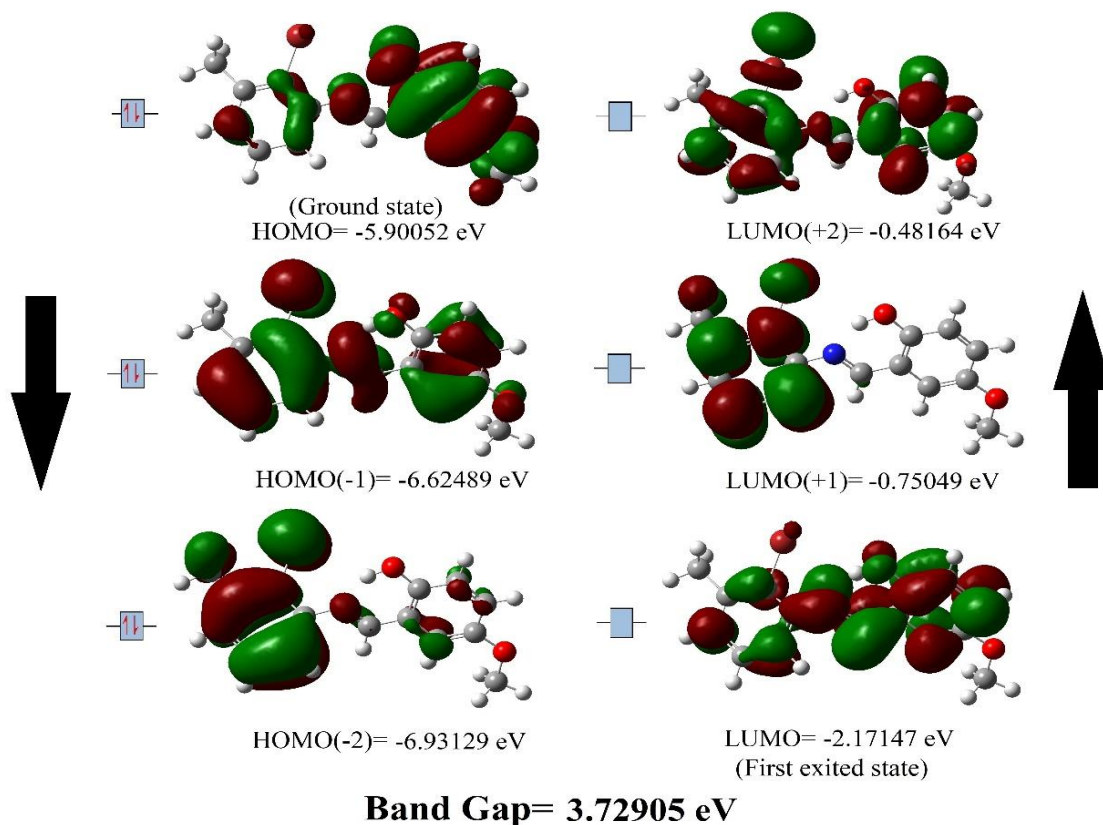
Band Gap= 3.72905 eV

Fig. 10: Frontier molecular orbitals of the studied molecule.

Table-5: Calculated net charges of the studied molecule.

| Atom	MPA	NPA	Atom	MPA	NPA
C1	-0.371493	-0.62817	C11	0.153798	-0.23948
C2	0.424157	-0.02149	C12	0.013655	-0.19639
C3	-0.870178	-0.20239	C13	-0.437455	0.29160
C4	0.079564	-0.18099	C14	-0.291457	-0.24711
C5	-0.149353	-0.22519	C15	-0.175061	-0.24255
C6	-0.052441	0.12009	O1	-0.541444	-0.67936
C7	0.251784	-0.13289	O2	-0.424328	-0.55512
C8	0.065968	0.15777	Br1	0.039575	0.05201
C9	0.186835	-0.16609	N1	-0.088549	-0.51208
C10	-0.451427	0.33175			
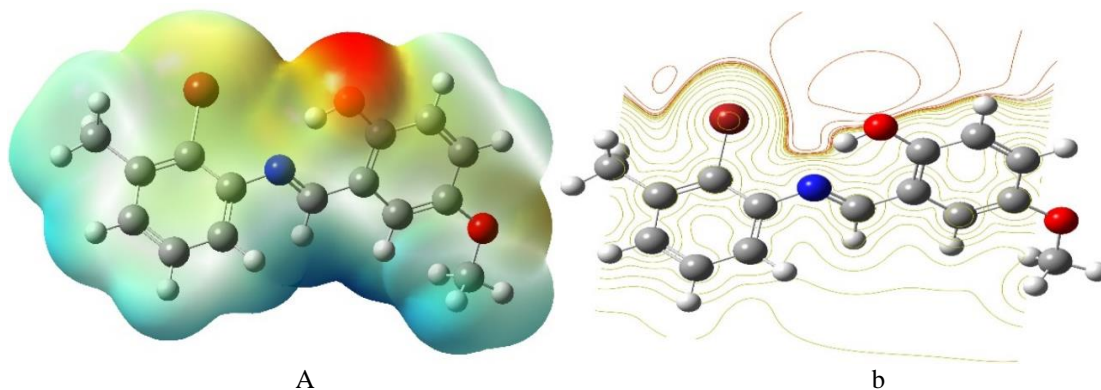
Fig. 11: (a) MEP surface. (b) Contour map for negative and positive potentials.

Molecular electrostatic potential

MEP analysis contributes in determining the electrophilic and nucleophilic sites in a reaction and identifying hydrogen bonding interactions. [58]. MEP surface map was generated using DFT at the same basis set to find the positive, negative, and neutral electrostatic potential regions of the studied molecule. The electrostatic potential contour map and surface map of the total electron density are shown in Fig. 11. The surface map uses colors, ranging from red to blue, to indicate different regions of the molecular electrostatic potential. Red, orange, or yellow regions represent high electron density and electronegative electrostatic potential (electrophilic attack), blue regions represent low electron density and positive electrostatic potential (nucleophilic attack), and green regions represent neutral potential [59, 60].

MEP surface of the title compound shows more nucleophilic attack than electrophilic attack (Fig. 11.a), while the MEP contour plot (Fig. 11.b) represents a 2D view of the relative electron density values at (0010).

Electrophilicity-based Charge Transfer method with DNA bases

The ECT calculation is used to know the direction of charge transfer. The ECT method helps study compounds and DNA bases that exhibit electron accepting or donating properties (electrophilic or nucleophilic behavior). If ECT value is positive, it indicates that the charges will be transferred from the base to the functional group, while if ECT value is negative, the charges will tend to transfer from the functional group to the base compound. [61].

IP and EA indicate to the ionization potential and electron affinity. These values are calculated based on neutral, anionic, and cationic species energy and referred in the equations below,

$$IP = [E(N - 1) - E(N)] \qquad (10)$$

$$EA = [E(N) - E(N + 1)] \qquad (11)$$

Electrophilicity refers to the ability of a chemical type to accept electrons from its environment. This is indicated by its negative electronic chemical potential, which must decrease upon accepting electrons. Nucleophilicity refers to a chemical substance's ability to donate electrons, which is revealed by a low electrophilicity nature. In a reaction between two molecules, the one with a lower electrophilicity index acts as a nucleophile [62]. The following formulae are used to determine ECT:

$$ECT = \left(\Delta N_{max}\right)_A - \left(\Delta N_{max}\right)_B \qquad (12)$$

$$\left(\Delta N_{max}\right)_A = \mu_A / \eta_A \text{ and } \left(\Delta N_{max}\right)_B = \mu_B / \eta_B \ (13)$$

Table-6. The calculated ECT values using DFT

	IP (eV)	EA (eV)	M (eV)	H (eV)	ΔN_{max}
Title compound	-0.38748	-7.38489	3.88619	3.49871	1.11075
Adenine ECT= 0.45110	2.14445	-10.4568	4.156185	6.30063	0.65965
Guanine ECT= 0,57177	3.386293	-11.304	3.95887	7.34517	0.53898
Cytosine ECT= 0.28406	0.880098	-9.27639	4.19814	5.07824	0.82669
Thymine ECT= 0.41545	2.0968	-11.6662	4.78469	6.88149	0.69529

In the case of DNA bases and the studied molecule, the electrons flow from the DNA bases to the molecule, making the DNA bases nucleophiles and the molecule an electrophile. The ECT value, which measures the difference in ΔNmax of the interacting molecules, was calculated as 0.45110, 0.57177, 0.28406, and 0.41545 eV for adenine, guanine, cytosine, and thymine, respectively (Table 6). As can be seen from previous results ECT > 0, therefore the electrons are transferred from DNA bases to the molecule. This indicates that the DNA bases act as donor while the compound acts as an acceptor.

FTIR spectroscopy

FTIR spectroscopy is a useful method for identifying the molecular composition of the compound. Fig. 12 displays the experimental IR spectrum of the studied compound. Table 7 lists some frequencies (in the range between 4000 - 450 cm^{-1}) of typical experimental values for the title compound and other reference values, as well as their probable assignments. Table 7 showing that the empirical values are in good agreement with the reference values [63].
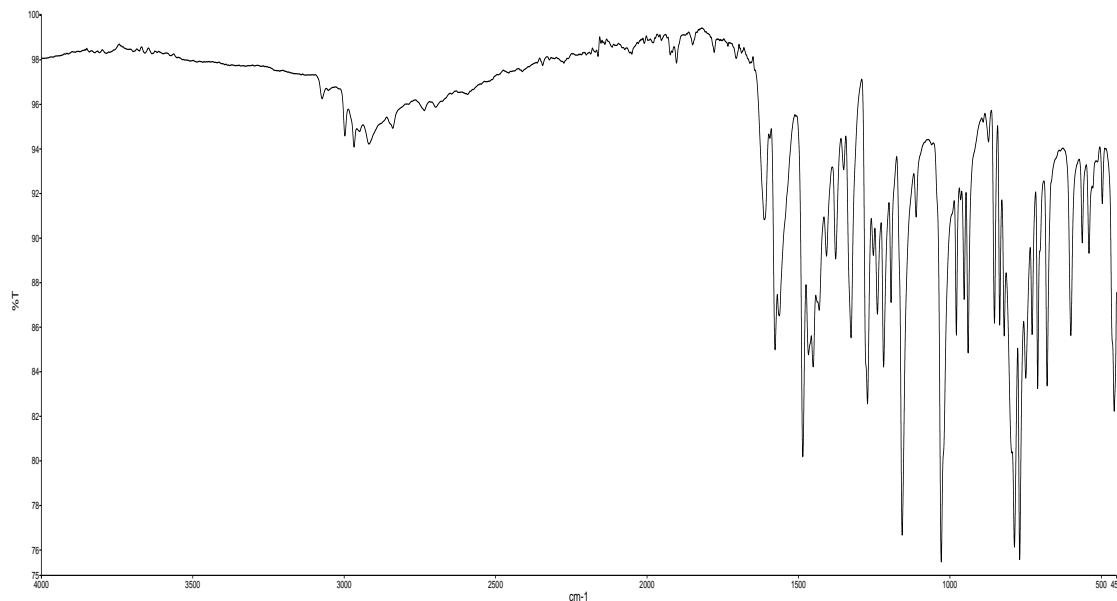
Usually, the aromatic compounds' C-H stretching modes value in absorption bands are between 3000–3100 cm^{-1} range [64]. In this study, the experimental C-H aromatic stretching mode was to be 3073 cm^{-1}. The alkyl CH3 vibration mode appeared at 2998 cm^{-1}. In the aromatic rings, the frequency values for the C=C and C-C bonds were observed at 1577 and 1272 cm^{-1}, respectively. The C=N stretching vibration was at 1612 cm^{-1}. The other vibration modes were displayed in Table 7.

Table-7: A comparison of experimental frequency values of the studied compound and reference values.

Assignment	Experimental (cm^{-1})	Reference value (cm^{-1})
v(O-H)	2500-3500	3414 [65]
v(C-H) aromatic	3073	3072 [66]
v(CH$_3$) stretching alkyl	2998	2998 [67]
v(CH$_3$)as methoxy	2968	2970 [68]
v(CH$_3$)s methoxy	2918	2924 [68]
v(C=N)	1612	1611 [69]
v(C=C) aromatic	1577	1573 [70]
v(C-C) aromatic	1272	1274 [70]
v(C-C)	1157	1155 [70]
v(Br-C)	979	977 [70]

Fig. 12: Experimental FTIR spectrum of the compound.

Conclusion

The studied compound was synthesized and analyzed using IR spectroscopy, X-ray single crystal diffraction and DFT. Results from X-ray data agreed well with DFT calculations using the B3LYP/6-311G++ basis set. According to the study of ECT, the electrons transferred from DNA bases to the considered compound indicating that DNA bases act as donor and the title molecule as acceptor, with DNA displaying nucleophilic behavior and the molecule showing electrophilic behavior. The HS and 2D fingerprint plots provided information on intermolecular interactions in the crystal, with the dominant forces being H...H (38%) and H...C/C...H (29%). MEP study revealed nucleophilic attack more than electrophilic attack. The chemical activity parameters indicated low intramolecular charge transfer, low chemical reactivity and high kinetic stability of the molecule.

References

1. H. Schiff, Mittheilungen aus dem Universitätslaboratorium in Pisa: Eine neue Reihe organischer Basen, *Ann. Chem. Pharm.*, **131**, (1864).

2. S.J. Almehmadi, A. Alharbi, M.M. Abualnaja, K. Alkhamis, M. Alhasani, S.H. Abdel-Hafez, R. Zaky, and N.M. El-Metwaly, Solvent Free Synthesis, Characterization, DFT, Cyclic Voltammetry and Biological Assay of Cu(II), Hg(II) and UO2(II) – Schiff Base Complexes, *Arab. J. Chem.*, **15**, (2022).

3. B.K. Kırca, Ç.A. Kaştaş and C.C. Ersanlı Molecular and Electronic Structures of Two New Schiff Base Compounds: (E)-2-Bromo-6-[(2-Bromo-4-Methylphenylimino) Methyl]-4-Chlorophenol and (E)-2-Bromo-6-[(4-Bromo-3-Methylphenylimino) Methyl]-4-Chlorophenol, *J. Mol. Struct.*, **1241**, (2021).

4. K.M. Chandini, F.H. Al-Ostoot, E.E. Shehata, N.Y. Elamin, H. Ferjani, M.A. Sridhar and N.K. Lokanath, Synthesis, Crystal Structure, Hirshfeld Surface Analysis, DFT Calculations, 3D Energy Frameworks Studies of Schiff Base Derivative 2,2′-((1Z,1′Z)-(1,2-Phenylene Bis(Azanylylidene)) Bis(Methanylylidene)) Diphenol, *J. Mol. Struct.*, **1244**, (2021).

5. A. Emriye, Synthesis and Characterization of Schiff Base 1-Amino-4-methylpiperazine Derivatives, *CBÜ Fen Bil. Dergi.*, **12**, (2016).

6. J.R. Anacona, J. Santaella, R.K.R. Al-Shemary, J. Amenta, A. Otero, C. Ramos and F. Celis, Ceftriaxone-Based Schiff Base Transition Metal(II) Complexes. Synthesis, Characterization, Bacterial Toxicity, and DFT Calculations. Enhanced Antibacterial Activity of a Novel Zn(II) Complex against S. Aureus and E. Coli, *J. Inorg. Biochem.*, **223**, (2021).

7. F.A. Almashal, M.Q. Mohammed, Q.M.A. Hassan, C.A. Emshary, H.A. Sultan and A.M. Dhumad, Spectroscopic and Thermal Nonlinearity Study of a Schiff Base Compound, *Opt. Mater.*, **100**, (2020).

8. S. Khani, M. Montazerozohori, R. Naghiha, Some Novel Nanostructure Schiff Base Compounds: Antimicrobial and Thermal Behaviors, *J. Phys. Org. Chem.*, **31**, 12, 3873 (2018).

9. Karrouchi, Khalid, Silvia A. Brandán, Mubashir Hassan, Khalid Bougrin, Smaail Radi, Marilena Ferbinteanu, Yann Garcia, and M'hammed Ansar, Synthesis, X-Ray, Spectroscopy, Molecular Docking and DFT Calculations of (E)-N'-(2,4-Dichlorobenzylidene)-5-Phenyl-1H-Pyrazole-3-Carbohydrazide, *J. Mol. Struct.*, **1228**, (2021).

10. T.H. Al-Noor, R.K. Mohapatra, M. Azam, L.K.A. Karem, P.K. Mohapatra, A.A. Ibrahim, P.K. Parhi, et al., Mixed-Ligand Complexes of Ampicillin Derived Schiff Base Ligand and Nicotinamide: Synthesis, Physico-Chemical Studies, DFT Calculation, Antibacterial Study and Molecular Docking Analysis, *J. Mol. Struct.*, **1229**, (2021).

11. A. Yildirim, F.A. Celik, M. Çıbuk, E. Yilmaz, Investigation of Bond Orientational Order of New Schiff Base and Theoretical Study on Covid-19 Activity: A Molecular Dynamics Based on DFT and Molecular Docking Analysis, *Chemical Physics Letters*, (2022).

12. H. Kargar, R. Behjatmanesh-Ardakani, V. Torabi, M. Kashani, Z. Chavoshpour-Natanzi, Z. Kazemi, V. Mirkhani, et al., Synthesis, Characterization, Crystal Structures, DFT, TD-DFT, Molecular Docking and DNA Binding Studies of Novel Copper(II) and Zinc(II) Complexes Bearing Halogenated Bidentate N,O-Donor Schiff Base Ligands, *Polyhedron*, **195**, 114988 (2021).

13. A.M. Fathi, H.S. Mandour, E. HassaneAnouar, Characteristics of Multidentate Schiff Base Ligand and Its Complexes Using Cyclic Voltammetry, Fluorescence, Antimicrobial Behavior and DFT-Calculations, *J. Mol. Struct.*, **1224**, (2021).

14. A.M. Abu-Dief, R.M. El-Khatib, F.S. Aljohani, S.O. Alzahrani, A. Mahran, M.E. Khalifa, N.M. El-Metwaly, Synthesis and Intensive Characterization for Novel Zn(II), Pd(II), Cr(III) and VO(II)-Schiff Base Complexes; DNA-Interaction, DFT, Drug-Likeness and Molecular Docking Studies, *J. Mol. Struct.*, **1242**, 130693 (2021).

15. S. Slassi, M. Aarjane, K. Yamni, A. Amine Synthesis, Crystal Structure, DFT Calculations, Hirshfeld Surfaces, and Antibacterial Activities of Schiff Base Based on Imidazole, *J. Mol. Struct.*, **1197**, (2019).

16. N. Süleymanoğlu, R. Ustabaş, Y.B. Alpaslan, U. Çoruh, S. Karakuş, S. Rollas, 2-Propylamino-5-[4-(2-Hydroxy-3,5-Dichlorobenzylideneamino) Phenyl]-1,3,4-Thiadiazole: X-Ray and DFT-Calculated Structures, *Struct. Chem.*, **21**, (2010).

17. E. Güzel, Z. Demircioğlu, C. Çiçek, E. Ağar, M. Yavuz, Experimental (XRD, FTIR, UV–Vis, NMR) and Theoretical Investigations (Chemical Activity Descriptors, NBO, DNA/ECT) of (E)-2-((2-Hydroxy-5-Methoxybenzylidene)Amino)-4-Nitrophenol, *Mol. Cryst. Liq. Cryst.*, **724**, (2021).

18. N. Süleymanoğlu, R. Ustabaş, Y. Ünver, Y.B. Alpaslan, Ş. Direkel, Ü. Karaman, 5-Phenyl Thiophene Amino Phenol Derivatives: Synthesis, Spectroscopic Characterization, Computational Study and Antimicrobial Activity, *J. Mol. Struct.*, **1182**, (2019).

19. A.A. Ağar, H. Tanak, M. Yavuz, Experimental and Quantum Chemical Calculational Studies on 2-[(4-Propylphenylimino)Methyl]-4-Nitrophenol, *Mol. Phys.*, **108**, (2010).

20. M. Kaur, H. Kaur, A. Kapila, Tautomerism, Spectroscopic and Computational Analysis of Schiff Base and Its Diphenyltin (IV) Complex, *J. Mol. Struct.*, **1185**, (2019).

21. G.M. Sheldrick, A Short History of SHELX, *Acta Crystallographica Section A Foundations of Crystlogr.*, **64**, (2008).

22. G.M. Sheldrick, Crystal Structure Refinement with SHELXL, *Acta Crystallographica Section C Struct. Chem.*, **71**, (2015).

23. L.J. Farrugia, WinGX Suite for Small-Molecule Single-Crystal Crystallography, *Journal of Applied Crystlogr.*, **32**, (1999).

24. L.J. Farrugia, WinGX and ORTEP for Windows : An Update, *Journal of Applied Crystlogr.*, **45**, (2012).

25. Mercury, Version 3.5.1; CCDC, available online via ccdc.cam.ac.uk/products/mercury. (2020).

26. A. L. Spek, Single-Crystal Structure Validation with the Program PLATON, *J. Appl. Crystallogr.*, **36**, (2003).

27. M. J. Frisch, "Gaussian09." http://www. gaussian. com/ (2009).

28. R., K., T. Dennington, (2009). GaussView, version 5.

29. L. P. Carrod, Antibiotic and Chemotherapy, 3rd ed. *Churchill Livingstone,Edinburgh*, **477**, (1972).

30. C. Lee, W. Yang, R.G. Parr, Development of the Colle-Salvetti Correlation-Energy Formula into a Functional of the Electron Density, *Phys. Rev. B*, **37**, (1988).

31. S. K. Wolff, (2012) Crystal Explorer 3.0. University of Western Australia, Perth.

32. N.K. Kaynar, H. Tanak, S. Şahin, N. Dege, E. Ağar, M. Yavuz, Molecular and Crystal Structure of 2-{(E)-[(4-Methylphenyl)Imino]Methyl}-4-Nitrophenol: A Redetermination, Cryst. Rep., **2**, (2016).

33. Ö. Bodur, G. Sevde, M. Yavuz, N. Dege, H. Bülbül, E. Ağar, (E)-2-{[(5-Chloro-2-Methoxyphenyl)Imino]Methyl}-4-Nitrophenol, IUCrData, **2**, (2017).

34. Z. Demircioğlu, Synthesis, Crystal Structure, Spectroscopic Characterization, Chemical Activity and Molecular Docking Studies of (E)-2-(((3-Chloro-4-Methylphenyl)Imino)Methyl)-6-Ethoxyphenol, J. Mol. Struct., **1246**, (2021).

35. I. Kılıç, E. Ağar, F. Erşahin, Ş. Işık, 2-[(4-Bromophenyl)Iminomethyl]-3,5-Dimethoxyphenol, *Acta Cryst. E*, **65**, (2009).

36. Ş. Atalay, S.N. Aygün, S. Meral, E. Ağar, (E)-4-Bromo-5-Methoxy-2-{[(2-Methoxyphenyl)Imino]Methyl}phenol Monohydrate, *IUCrData*, **2**, (2017).

37. G.A. El-Hiti, K. Smith, M. Alamri, C.A. Morris, P. Kille, B.M. Kariuki, 5-Bromo-1-(4-Bromophenyl)Isatin, *IUCrData*, **3** (2018).

38. H. Tanak, A. Ağar, M. Yavuz, Combined Experimental and Computational Modeling Studies on 4-[(2-Hydroxy-3-Methylbenzylidene) Amino]-1,5-Dimethyl-2-Phenyl-1,2-Dihydro-3H-Pyrazol-3-One: Combined Experimental and Computational Modeling Studies, Int. J. Quantum Chem., **111**, (2011).

39. Ş. Atalay, S. Gerçeker, S. Meral, H. Bülbül, 2-{(E)-[(3-Chloro-4-Methyl-phen-yl)Imino]-meth-yl}-4-(Tri-fluoro-meth-oxy)Phenol, IUCrData, **2**, (2017).

40. M. Hassan, Z. Ashraf, S.Y. Seo, D. Kim, S.K. Kang, Crystal Structure of 5-Hydroxymethyl-2-Methoxyphenol, Acta Cryst. E, **71**, (2015).

41. [B. Inturi, K.R. Roopashree, G.V. Pujar, I.A. Mohammed, H.C. Devarajegowda, 2-Methoxy-4-[3-(3-Nitrophenyl)-4,5-Dihydro-1 H -Pyrazol-5-Yl]Phenol, IUCrData, **1**, (2016).

42. S.B. Nasir, Z. Abdullah, Z.A. Fairuz, S.W. Ng, E.R.T. Tiekink, 2-(4-Methoxyphenoxy)-3-Nitropyridine, Acta Cryst. E, **66**, (2010).

43. M.A. Spackman, D. Jayatilaka, Hirshfeld Surface Analysis, Cryst. Eng. Comm., **11**, (2009).

44. Z. Demircioğlu, C.C. Ersanli, S. Şaşmaz, Spectroscopic, Hirshfeld Surface, X-Ray Diffraction Methodologies and Local & Global Chemical Activity Calculations of 5-(2-Methoxy-

4-(Prop-1-En-1-Yl)Phenoxy)Pyrazine-2,3-Dicarbonitrile, J. Mol. Struct., **1181**, (2019).

45. S. Kansız, A. Tolan, M. Azam, N. Dege, M. Alam, Y. Sert, S.I. Al-Resayes, H. İçbudak, Acesulfame Based Co(II) Complex: Synthesis, Structural Investigations, Solvatochromism, Hirshfeld Surface Analysis and Molecular Docking Studies, Polyhedron, **218**, (2022).

46. S. Janeoo, A. Saroa, R. Kumar, H. Kaur, Computational Investigation of Bioactive 2,3-Diaryl Quinolines Using DFT Method: FT- IR, NMR Spectra, NBO, NLO, HOMO-LUMO Transitions, and Quantum-Chemical Properties, J. Mol. Struct., **1253**, (2022).

47. A. Ouaket, A. Chraka, I. Raissouni, M.A. El Amrani, M. Berrada, N. Knouzi, Synthesis, Spectroscopic (13C/1H-NMR, FT-IR) Investigations, Quantum Chemical Modelling (FMO, MEP, NBO Analysis), and Antioxidant Activity of the Bis-Benzimidazole Molecule, J. Mol. Struct., **1259**, (2022).

48. B. Khan, M. Khalid, M.R. Shah, M.N. Tahir, M.U. Khan, A. Ali, S. Muhammad, Efficient Synthesis by Mono-carboxy Methylation of 4,4′-biphenol, X-ray Diffraction, Spectroscopic Characterization and Computational Study of the Crystal Packing of Ethyl 2-((4′-hydroxy-[1,1′-biphenyl]-4-yl)Oxy)Acetate, Chem. Sel., **32**, (2019).

49. M. Missioui, S. Mortada, W. Guerrab, G. Demirtaş, J.T. Mague, M.E.A. Faouzi, et al., Greener Pastures in Evaluating Antidiabetic Drug for a Quinoxaline Derivative: Synthesis, Characterization, Molecular Docking, in Vitro and HSA/DFT/XRD Studies, Arab. J. Chem., **15**, (2022).

50. H. Jafari, I. Danaee, H. Eskandari, M. RashvandAvei, Electrochemical and Theoretical Studies of Adsorption and Corrosion Inhibition of N,N′-Bis(2-Hydroxyethoxyacetophenone)-2,2-Dimethyl-1,2-Propanediimine on Low Carbon Steel (API 5L Grade B) in Acidic Solution, Ind. Eng. Chem. Res., 52, **20**, (2013).

51. M. Agrawal, V. Deval, A. Gupta, B.R. Sangala, S.S. Prabhu, Evaluation of Structure-Reactivity Descriptors and Biological Activity Spectra of 4-(6-Methoxy-2-Naphthyl)-2-Butanone Using Spectroscopic Techniques, Spectrochimica Acta Part A: Mol. Biomol. Spectrosc., **167**, 142–56 (2016).

52. T. Koopmans, Über die Zuordnung von Wellenfunktionen und Eigenwerten zu den Einzelnen Elektronen Eines Atoms, Physica, **1**, (1934).

53. S. Uzun, Z. Demircioğlu, M. Taşdoğan, E. Ağar, Quantum Chemical and X-Ray Diffraction Studies of (E)-3-(((3,4-Dimethoxybenzyl)Imino)Methyl)Benzene-1,2-Diol, J. Mol. Struct., **1206**, (2020).

54. G. Dikmen, İ. Kani, Synthesis, Spectroscopic Characterization (FT-IR, Raman, UV-VIS, XRD), DFT Studies and DNA Binding Properties of [Ni(C6H5CH2COO)(C12H8N2)2](ClO4)(CH3OH) Compound, J. Mol. Struct., **1209**, (2020).

55. Z. Gültekin, Z. Demircioğlu, W. Frey, O. Büyükgüngör, A Combined Experimental (XRD, FT-IR, UV-VIS and NMR) and Theoretical (NBO, NLO, Local & Global Chemical Activity) Studies of Methyl 2-((3R,4R)-3-(Naphthalen-1-Yl)-4-(Phenylsulfonyl) Isoxazolidin-2-Yl) Acetate, J. Mol. Struct., **1199**, 126970 (2020).

56. G. Rajarajan, V. Thanikachalam, S. Selvanayagam, B. Sridhar, Synthesis, Spectroscopic (UV–Vis, FT-IR and NMR), Single Crystal XRD of 3,5-Diethyl -2,6-Di(Thiophen-2-Yl)Piperidin-4-on-1-Ium Picrate: A Comprehensive Experimental and Computational Study, J. Mol. Struct., **1128**, (2017).

57. Z. Demircioğlu, Ç.A. Kaştaş, O. Büyükgüngör, XRD, FT–IR and UV Characterization, Hirshfeld Surface Analysis and Local-Global Chemical Descriptor Studies of (E)-2-((3-Fluorophenylimino)Methyl)-3-Methoxyphenol (1) and (E)-2-((2-Fluorophenylimino)Methyl)-3-Methoxyphenol (2), J. Mol. Struct., **1166**, (2018).

58. K.E. Srikanth, A. Veeraiah, T. Pooventhiran, R. Thomas, K.A. Solomon, C.J.S. Raju, J.N.L. Latha, Detailed Molecular Structure (XRD), Conformational Search, Spectroscopic Characterization (IR, Raman, UV, Fluorescence), Quantum Mechanical Properties and Bioactivity Prediction of a Pyrrole Analogue, Heliyon, **6**, (2020).

59. S.B. Radder, R. Melavanki, S.M. Hiremath, R. Kusanur, S.S. Khemalapure, S.C. Jeyaseelan, Synthesis, Spectroscopic (FT-IR, FT-Raman, NMR & UV-Vis), Reactive (ELF, LOL, Fukui), Drug Likeness and Molecular Docking Insights on Novel 4-[3-(3-Methoxy-Phenyl)-3-Oxo-Propenyl]-Benzonitrile by Experimental and Computational Methods, Heliyon, **7**, (2021).

60. E. İnkaya, Synthesis, X-Ray Structure, FT-IR, NMR (13C/1H), UV–Vis Spectroscopy, TG/DTA Study and DFT Calculations on 2-(Benzo[d]Thiazol-2-Ylthio)-1-((1s, 3s)-3-Mesityl-3-Methylcyclobutyl) Ethan-1-One, J. Mol. Struct., **1173**, (2018).

61. S. Çakmak, S. Kansiz, M. Azam, C.C. Ersanlı, O. İdil, A. Veyisoğlu, H. Yakan, H. Kütük, A. Chutia, Synthesis, Structural Investigation,

Hirshfeld Surface Analysis, and Biological Evaluation of N -(3-Cyanothiophen-2-Yl)-2-(Thiophen-2-Yl)Acetamide, ACS Omega, **7**, 13, 11320–29 (2022).

62. Ö. Ekici, Z. Demircioğlu, C.C. Ersanlı, A. Çukurovalı, Experimental and Theoretical Approach: Chemical Activity, Charge Transfer of DNA/ECT, Thermodinamic, Spectroscopic, Structural and Electronic Properties of N-(4-(3-Methyl-3-Phenylcyclobutyl)Thiazol-2-Yl)Acetamide Molecule, J. Mol. Struct., **1204**, (2020).

63. H.T. Akçay, U. Çoruh, R. Bayrak, E. Menteşe, E.M.V. Lopez, A Spectroscopic Study on New Phthalonitrile Derivative and Its Computational Background: 4-[(4,5-Diphenyl-4H-1,2,4-Triazol-3-Yl)Sulfanyl]Benzene-Phthalonitrile, J. Mol. Struct., **1127**, 539–48 (2017).

64. Z. Demircioğlu, G. Kaştaş, Ç.A. Kaştaş, R. Frank, Spectroscopic, XRD, Hirshfeld Surface and DFT Approach (Chemical Activity, ECT, NBO, FFA, NLO, MEP, NPA& MPA) of (E)-4-Bromo-2-[(4-Bromophenylimino)Methyl]-6-Ethoxyphenol, J. Mol. Struct., **1191**, (2019).

65. N. Süleymanoğlu, R. Ustabaş, Y. Ünver, Y.B. Alpaslan, Ş. Direkel, Ü. Karaman, 5-Phenyl Thiophene Amino Phenol Derivatives: Synthesis, Spectroscopic Characterization, Computational Study and Antimicrobial Activity, J. Mol. Struct., **1182**, 36–46 (2019).

66. G. Demirtaş, N. Dege, E. Ağar, S.G. Uzun, The Crystallographic, Spectroscopic and Theoretical Studies on (E)-2-(((4-Chlorophenyl)Imino)Methyl)-5-(Diethylamino)Phenol and (E)-2-(((3-Chlorophenyl)Imino)Methyl)-5-(Diethylamino)Phenol Molecules, J. Mol. Struct., **1152**, (2018).

67. E. Güzel, Z. Demircioğlu, C. Çiçek, E. Ağar, Experimental and Theoretical Approach: Local and Global Chemical Activity, Charge Transfer Method with DNA Bases, Spectroscopic, Structural and Electronic Properties of (E)-2-(((4-Fluorophenyl)Imino)Methyl)-4-Methoxyphenol, J. Mol. Struct., **1204**, (2020).

68. Ü. Ceylan, G.Ö. Tarı, H. Gökce, E. Ağar, Spectroscopic (FT–IR and UV–Vis) and Theoretical (HF and DFT) Investigation of 2-Ethyl-N-[(5-Nitrothiophene-2-Yl)Methylidene]Aniline, J. Mol. Struct., **1110**, 1–10 (2016).

69. H. Gökce, Y.B. Alpaslan, C.T. Zeyrek, E. Ağar, A. Güder, N. Özdemir, G. Alpaslan, Structural, Spectroscopic, Radical Scavenging Activity, Molecular Docking and DFT Studies of a Synthesized Schiff Base Compound, J. Mol. Struct., **1179**, (2019).

70. İ. Bozkurt, M. Evecen, H. Tanak, E. Ağar, Spectroscopic and Electronic Properties of 4-Bromo-5-Fluoro-2-((3-Nitrophenylimino)Methyl)Phenol Schiff-Base Molecule: Experimental and Theoretical Investigations, J. Mol. Struct., **1197**, (2019).